Analytical Letters

ISSN: 0003-2719 (Print) 1532-236X (Online) Journal homepage: www.tandfonline.com/journals/lanl20

Detecting Cardiovascular Diseases and Diabetes Mellitus Through Fingernails Using Attenuated Total Reflectance-Fourier Transform Infrared Spectroscopy and Machine Learning

Megan Wilson, Dhiya Al-Jumeily, Leung Tang, Jason Birkett, Iftikhar Khan, Ismail Abbas & Sulaf Assi

To cite this article: Megan Wilson, Dhiya Al-Jumeily, Leung Tang, Jason Birkett, Iftikhar Khan, Ismail Abbas & Sulaf Assi (27 Jul 2025): Detecting Cardiovascular Diseases and Diabetes Mellitus Through Fingernails Using Attenuated Total Reflectance-Fourier Transform Infrared Spectroscopy and Machine Learning, Analytical Letters, DOI: 10.1080/00032719.2025.2534604

To link to this article: https://doi.org/10.1080/00032719.2025.2534604

Published online: 27 Jul 2025.

ANALYTICAL LETTERS
https://doi.org/10.1080/00032719.2025.2534604

Taylor & Francis
Taylor & Francis Group

INFRARED

Detecting Cardiovascular Diseases and Diabetes Mellitus Through Fingernails Using Attenuated Total Reflectance-Fourier Transform Infrared Spectroscopy and Machine Learning

Megan Wilson[a], Dhiya Al-Jumeily[b], Leung Tang[c], Jason Birkett[a], Iftikhar Khan[a], Ismail Abbas[d], and Sulaf Assi[a]

[a]School of Pharmacy and Biomedical Sciences, Liverpool John Moores University, Liverpool, United Kingdom; [b]School of Computer Science and Mathematics, Liverpool John Moores University, Liverpool, United Kingdom; [c]Chemical Analysis Group, Agilent Technologies, United Kingdom; [d]Faculty of Science, Lebanese University, Beirut, Lebanon

ABSTRACT

Cardiovascular diseases (CVDs) and diabetes mellitus (DM) represent a global concern for the public and often result in severe medical and/or economic consequences. Traditional disease detection techniques such as blood work and cardiac catheterization are not only invasive and intrusive, but also require high expenses for equipment, facilities and training. This urges for the use of alternative methods such as infrared (IR) spectroscopy, which has shown great success in the detection of cancer, Fabry disease and kidney disease. Through the combination of machine learning algorithms (MLAs) and the alternative biological matrices (fingernails), infrared (IR) spectroscopy has the potential to replace traditional techniques, especially in low- and middle-income countries, where the economic and medical consequences created by CVDs and DM are at their highest. Thus, this work explored the detection of CVDs and DM through fingernails using attenuated total reflectance-Fourier transform infrared (ATR-FTIR) spectroscopy, chemometrics and MLAs such as correlation in wavenumber space (CWS), principal component analysis (PCAs) and self-organizing maps (SOMs). Spectral interpretation of fingernail spectra revealed the presence of key endogenous compounds such as amino acids, lipids and proteins, as well as disease-related compounds including glucose, high-density lipoproteins (HDLs) and homocysteine. Moreover, the applied MLAs demonstrated the feasibility of ATR-FTIR spectroscopy for the classification of healthy vs. diseased fingernails. Of these MLAs, PCA and SOM were more accurate than CWS where the latter showed high number of mismatches between fingernail spectra of varying health/disease status. However, PCA and SOM demonstrated more accurate clustering between healthy and diseased fingernails. This in turn confirmed that ATR-FTIR and MLAs were accurate in detecting CVDs and DM in fingernails non-destructively.

ARTICLE HISTORY
Received 16 May 2025
Accepted 11 July 2025

KEYWORDS
Attenuated total reflectance-Fourier transform infrared spectroscopy (ATR-FTIR); cardiovascular diseases; diabetes mellitus; fingernails; machine learning

CONTACT Megan Wilson m.wilson3@2019.ljmu.ac.uk School of Pharmacy and Biomedical Sciences, Liverpool John Moores University, Byrom Street, Liverpool L3 3AF 3, United Kingdom.

Introduction

The incidence of cardiovascular diseases (CVDs) represents a global concern for the public. Collectively CVDs have remained the leading cause of death globally and have created severe medical and economic consequences (World Health Organisation 2019). In 2019, the number of CVD deaths was approximately 17.9 million and this number is expected to rise to 23.6 million in 2030, if their diagnosis and treatment is not vastly improved (Ghazali et al. 2015; Roman, Martin, and Sauli 2019; Vaduganathan et al. 2022; World Health Organisation 2019). The rise of CVD cases has become detrimental in low- and middle-income countries (LMICs) in comparison to developed countries, where treatment and diagnostic training are more accessible (Sianga, Mbago, and Msengwa 2025). Through the rise in risk factors including excessive alcohol consumption, poor exercise and smoking, CVDs now do not only affect older people, but also young individuals, who are more likely to take part in risk factors/behaviors (Dedefo et al. 2018). The accessibility of such risk factors/behaviors have now created a paradigm shift within the prevalence of disease.

A close link exists between CVDs and diabetes mellitus (DM), which is also extremely prevalent in LMICs (Leon and Maddox 2015). In fact, CVDs are the most prevalent cause of mortality and morbidity within the diabetic population (Leon and Maddox 2015; Matheus et al. 2013). Moreover, direct costs related to DM primarily lend themselves to macrovascular and microvascular complications such as coronary artery disease (CAD), hypertension, myocardial infarction and peripheral vascular disease (American Diabetes Association 2008; Bahia et al. 2011). To minimize the prevalence of such diseases and their economic burden, it is first crucial that diagnostic errors are avoided. Diagnostic errors, characterized by the late or misdiagnosis of disease, are under-recognized sources of patient harm and excessive spending linked to malpractice litigation cases and the administration of unnecessary treatment/therapies (Gandhi et al. 2006; Phillips et al. 2004; Quinn et al. 2017; Schiff et al. 2013; Zuccotti and Sato 2011). The diagnosis of CVDs and/or DM can often be challenging, particularly in patients who do not take part in risk factor behaviors or present atypical disease symptoms (Panju et al. 1998; Quinn et al. 2017; Sequist et al. 2006, 2012). For example, a previous systematic review identified sex bias within the diagnosis of CVDs in females. The diagnosis of CVDs for female patients is difficult, as females often display atypical symptoms that are misdiagnosed as anxiety or gastrointestinal related (Al Hamid et al. 2024). As a result, CVDs are often left untreated and further complications arise such as angina and stroke, as well other comorbidities including DM and depression (Thompson and Yancy 2004).

Another study reported the extreme misclassification of DM, with 10–25% of patients with type 2 diabetes mellitus (T2DM) being incorrectly diagnosed with type 1 diabetes mellitus (T1DM) (Lusignan et al. 2010, 2011). Additionally, another 5% of patients diagnosed with T2DM showed no objective evidence of DM (Lusignan et al. 2010, 2011). Therefore, to improve the economic burden created through the misdiagnosis of CVDs and/or DM, disease detection techniques must be highly sensitive.

Traditional techniques for the detection of CVDs and/or DM include blood work, cardiac catheterization, cardiac stress testing, chest X-rays, computed topography (CT) scans and echocardiogram (ECGs) (American Diabetes Association 2011; Bangalore

et al. 2021; Gillam and Marcoff 2024; Ladapo, Blecker, and Douglas 2010; Lopez-Mattei et al. 2023). While the aforementioned techniques do offer high sensitivity, there use in LMICs in often unfeasible. For example, interpretation of CT scans and ECGs require advanced user knowledge (Amini et al. 2022; Kazemi et al. 2023). In LMICs were training and equipment maintenance is expensive, such methods are not plausible. Therefore, interpretations can after create misdiagnosis, mistreatment and create additional disease-related complications.

New techniques are thus required to deliver accurate accounts of disease detection, with a high degree of sensitivity and specificity. Infrared (IR) spectroscopy, which is based on the scattering, reflection, absorption or transmission of IR radiation, offers affordable, non-intrusive and noninvasive analysis of a range of biological matrices including blood (plasma and serum), fingernails, hair, urine and saliva (Jee 2024). ATR-FTIR spectroscopy has been shown to be successful in detecting diseases from different biological matrices including saliva (Jee 2024; Kumar, Srinivasan, and Nikolajeff 2018), serum (Silva et al. 2024) and fingernails (Coopman et al. 2017; Farhan, Sastry, and Mandal 2011). The aforementioned studied demonstrated the potential for ATR-FTIR in detecting diseases by monitoring biomarkers and/or endogenous compounds in biological matrices. Endogenous compounds reported were lipids, proteins and sugars (Coopman et al. 2017; Farhan, Sastry, and Mandal 2011; Jee 2024; Kumar, Srinivasan, and Nikolajeff 2018; Silva et al. 2024; Wu et al. 2023). Particularly in fingernails, keratin glycation was monitored using ATR-FTIR spectroscopy (Coopman et al. 2017; Farhan, Sastry, and Mandal 2011). Yet, some confounding factors related to other diseases affected the glycation process in the study.

Considering these limitations, the present study built on the findings of the latter study (Coopman et al. 2017; Farhan, Sastry, and Mandal 2011) in applying ATR-FTIR spectroscopy to individuals that have DM co-existing with other conditions, e.g., CVDs. Thus, the present study evaluated the signature of fingernails in multiple conditions and utilized unsupervised machine learning algorithms (MLAs) to understand differences in healthy and diseased fingernails.

MLAs have showed advancement in previous studies by significantly improving the efficiency of analyzing ATR-FTIR spectra from biological samples; thus, facilitating clinical applications including screening, diagnosis, risk stratification and prognosis prediction of Alzheimer's disease, aspergillosis, cancer, Covid-19, hepatitis C virus, malaria and paracoccidioidomycosis (Alajaji et al. 2025; Coopman et al. 2017; Fadlelmoula et al. 2023; Farhan, Sastry, and Mandal 2011; Maiti 2023; Wu et al. 2023). Therefore, this study built on the previous studies that used either ATR-FTIR spectroscopy and/or MLAs for diseases diagnosis. As such, this study explored the detection of CVDs and DM through fingernails using ATR-FTIR spectroscopy and MLAs.

Methodology

Sample collection

Ethical approval for the collection of fingernail clippings was granted by two institutes, those being: Liverpool John Moores University (LJMU) (23/PBS/009A) and the Lebanese University (2022-0104). Participants were approached through a LJMU's

community site and were provided with a participant information sheet, questionnaire and consent form. Inclusion criteria included adult age (≥18 years old), while those that were <18 years old were excluded from the study. Individuals, with no previous medical diagnosis, were included and classed as healthy controls. Those that had a previous diagnosis of a medical condition or disease, which was not related to either CVDs or DM, were accepted but classified as unhealthy away from the CVD and/or diabetic participants. Moreover, those with a CVD such as hypertension or CAD and/or DM (type 1 or type 2), were included and classified as either CVD, diabetic or CVD-diabetic. The optimized sample size was calculated through the following equation for the sample size (Al Hamid 2015):

$$n = \frac{t^2 x\ p(1-p)}{m^2} \tag{1}$$

where n is the desired sample size, t represents the level of confidence at 95% (1.96), p is the estimated prevalence of the characteristics of interest in the project area, and m is the error margin at 5% (0.05).

Based on Eq. (1) and considering the previous studies, an ideal sample size of 381 fingernail clippings was sought. As 126 participants were recruited, 1182 fingernail clippings were accounted for, as several participants failed to provide a full set ($n = 10$). In this respect, 92 (73%) sets of fingernails were complete, 15 (12%) sets had nine clippings, eight sets (6%) had eight clippings, six (5%) had seven clippings and five (4%) had six clippings. Fingernail clippings where then stored in 2 mL glass vials prior to analysis. Participants were also asked to fill in an anonymous questionnaire for the collection of clinical data, which complemented the IR data.

The sample consisted of both female ($n = 76$, 60%) and male ($n = 50$, 40%) participants, aged between 18 and 84 years old. Across this age range, participants were categorized into five age groups, those being: 18–24 ($n = 21$, 17%), 25–34 ($n = 11$, 9%), 35–39 ($n = 5$, 4%), 40–64 ($n = 69$%, 55%) and 65–84 ($n = 20$, 16%) years old. A total of seven ethnic groups were represented and included Arab ($n = 38$, 30%), Asian ($n = 14$, 11%), Indian ($n = 2$, 2%), Lebanese Arab ($n = 22$, 17%), Middle Eastern Arab ($n = 2$, 2%), mixed (unspecified) ($n = 2$, 2%) and White ($n = 46$, 37%). Based on the clinical data provided and the participants health or disease status, participants were placed into one of five groups those being healthy ($n = 68$, 53.9%), other unhealthy (medical condition that is not CVD and/or DM) ($n = 23$, 18.7%), CVD ($n = 15$, 11.9%), diabetic ($n = 5$, 3.97%) and CVD-diabetic ($n = 15$, 11.9%). CVD participants reported the presence of atrial fibrillation ($n = 1$, 6.67%), heart disease ($n = 2$, 13.3%) and hypertension ($n = 12$, 80%). The diabetic participants reported either type 1 (T1DM) ($n = 1$, 20%) or type 2 diabetes mellitus (T2DM) ($n = 4$, 80%).

Prior to spectral measurements, the length, depth and width of each fingernail clipping was taken. Based on these measurements, each fingernail clipping received a label of A–J. Fingernails labeled A and B, were the largest in length and were usually taken from the thumb. While fingernail clippings I and J were the smallest fingernail clipping and taken from the participant's little finger.

Instrumentation

For the collection of ATR-FTIR spectra, the Agilent 4500a ATR-FTIR spectrometer was utilized (Agilent Technologies, Inc. Santa Clara, CA). Samples were measured over the range 4000–650 cm^{-1} using an ATR diamond and diamond holder. At a resolution of 4 cm^{-1}, 64 backgrounds scans were taken per spectrum. Apodization was carried out using a triangular motion.

Fingernail measurements

Prior to measurements being taken, fingernail clippings were removed from clear glass vials. In cases of contamination such as fingernail polish and/or environmental dirt, fingernails were soaked in acetone for 2–3 h. For the collection of ATR-FTIR spectra, individual fingernail clippings were placed directly onto the diamond holder and held into place using the presser. The applied pressure ensured that the fingernail clipping was flat against the ATR diamond. For each clipping, a total of three spectra were taken, hence, producing 30 spectra per fingernail set. To ensure maximized spectral collection and that the distribution of the endogenous compound across was accounted for, spectra were collected from the dorsal and ventral layers. When fingernail sets were incomplete (<10 fingernails clippings), additional spectra were collected. In between spectra, the ATR diamond was cleaned and a background taken. A reference spectrum of polystyrene film was also used for calibration purposes and to return the instrument to its original baseline. Thus, reference spectra were taken before and after the application of fingernails.

Data analysis

For spectral visualization and application MLAs, ATR-FTIR spectra were imported into MATLAB 2019a. The aforementioned software allowed for the visualization of ATR-FTIR spectra for the purpose of spectral quality and spectral interpretation assessments. Spectral quality parameters included number of bands, maximum band position/intensity, range and the signal-to-noise ratio. The highlighted parameters were utilized to determine the IR activity as either strong, medium or weak.

To further explore the feasibility of ATR-FTIR spectrometry, MLAs such as correlation in wavenumber space (CWS), principal component analysis (PCA) and self-organizing maps (SOMs) were employed. The application of CWS allowed the correlation coefficient (r) values of the test spectrum to be matched against the reference spectrum (Assi et al. 2019). A calculated r value of −1 indicated that the test and reference spectra were completely dissimilar. While an r value of +1 demonstrated that the test and reference spectra were identical. Due to sample noise, it was often difficulty to obtain an r value of +1; therefore a threshold of 0.95 was employed as a match (Assi et al. 2019).

To reduce the original matrix's dimensionality into subspaces of scores and loadings, PCA was applied. The PC scores demonstrated the distribution of fingernails, particularly healthy vs. diseased fingernails, in a multidimensional space. Additionally, the PC scores allowed for the visualization of clusters and pattern within the dataset (Abid et al. 2018). In this respect, clustering scores of the healthy fingernails away from the

diseased or unhealthy fingernails. The PC loadings demonstrated significant absorbance values that were representative of key endogenous compounds found within the fingernails (Jolliffe and Cadima 2016). As a linear combination of the original data, PCs were calculated and ordered based on their size. Thus, the first dimension (PC1) provided explainability for the highest variance, followed by the second dimension (PC2) for the second highest variance and the third dimension (PC3) for the third highest dimension (Camargo 2022). To validate the PCA findings, SOMs were employed. As neural network modes, SOMs were composed of organized neurons that could detect spectral features without an awareness of spectra's classes or memberships (Assi et al. 2023). Based on previous experiments, three variations were expected within the SOMs, including the fingernail's physical properties, fingernail's water content and the absence or presence of disease, a 3×3 SOM was applied with 100 epochs.

Results and discussion

Spectral analysis of fingernails

Spectral interpretation of 126 fingernail sets ($n = 1191$ fingernail clippings) was carried out and represented healthy, unhealthy, CVD, diabetic and CVD-diabetic participants. A comparison with the literature and reference standards revealed key ATR-FTIR frequencies and their corresponding endogenous compounds (Table 1).

Several amide groups were identified over the 4000–650 cm^{-1} range. Amide A of the fingernail's protein was identified at 3277 cm^{-1} and was attributed to symmetric N–H stretching (Selvam and Gunasekaran 2018). Amide A and B were detected at 3067 cm^{-1} and were related to N–H stretching (Sharma et al. 2020).The presence of Amide I was identifiable at 1642 cm^{-1} and related to C=O stretching coupled with in-plane bending of N–H and C–N stretching of the fingernails' α-helix (Sundaram et al. 2016). Amide II was detected between the region 1582–1562 and at 1535 cm^{-1} and was attributed N–H in-plane bending, coupled with C–N stretching vibrations of proteins and C–O stretching coupled with N–H bending deformation and C–H stretching, respectively (Gunasekaran et al. 2010). Finally, amide III was detected at 1296 and 1249 cm^{-1}, which were attributed to N–H bending and N–H in plane bending paired with O=C–N bending and C–N stretching, respectively (Sharma et al. 2020).

The presence of lipids was identified at 2960 cm^{-1} and were related to C–H asymmetric stretching of CH_3 (Sharma et al. 2020; Sundaram et al. 2016). Lipids and proteins were also detected at 2920, 2851 and 1452 cm^{-1}, which was attributed to C–H symmetric stretching of CH_3, C–H symmetric stretching of CH_2 and CH_2 and CH_3 asymmetric bending modes (Sharma et al. 2020; Sundaram et al. 2016). At 1738 cm^{-1}, high-density lipoproteins were identified and was associated with the C=O groups of cholesterol esters (Selvam and Gunasekaran 2018; Gunasekaran et al. 2010).

Several amino acids were detected at 1398 cm^{-1} and included cysteine, cystine, tyrosine and tryptophan (symmetric mode of CH_3) (Barton 2004; Bantignies et al. 1998). Interestingly, glucose was identifiable at key bands 1115 and 1080 cm^{-1} and were attributed to stretching of glycogen and CO symmetric stretching, respectively (Abid et al. 2018).

Table 1. Spectral interpretation of healthy, unhealthy, CVD, diabetic and CVD-diabetic participants measured using the Agilent 4500a ATR-FTIR spectrometer equipped with an ATR diamond.

Band position (cm^{-1})	Functional group	Association
3277	Symmetric N–H stretching	Amide A of protein (Selvam and Gunasekaran 2018)
3067	N–H stretching	Amide A and B (Sharma et al. 2020)
2960	C–H asymmetric stretching of CH_3	Lipids and total cholesterol (Sharma et al. 2020; Sundaram et al. 2016)
2920	C–H symmetric stretching of CH_3	Lipids and proteins (Sundaram et al. 2016)
2851	C–H symmetric stretching in CH_2	Lipids and proteins (Sundaram et al. 2016)
1738	C=O groups of cholesterol esters	High-density lipoproteins (Gunasekaran et al. 2010; Selvam and Gunasekaran 2018)
1644–1642	C=O stretching coupled with in-plane bending of N–H and C–N stretching	Amide I (α-helix) (Farhan, Sastry, and Mandal 2011; Mitu et al. 2023; Sundaram et al. 2016)
1633	C=O stretching	Amide I (Sundaram et al. 2016)
1582–1562	N–H in plane bending vibration strongly coupled to C–N stretching vibration protein, NH_2 scissoring	Amide II, homocysteine (Gunasekaran et al. 2010)
1535	C=O stretching coupled with C–N stretching and bending deformation of N–H	Amide II (Sundaram et al. 2016)
1452	CH_2 and CH_3 asymmetric bending modes	Lipids and proteins (Sharma et al. 2020; Sundaram et al. 2016)
1447	Methyl symmetric deformation	Amino acids, triglycerides (Fernández-Higuero et al. 2014)
1398	Symmetric mode of CH_3	Amino acids (Bantignies et al. 1998; Barton 2004)
1296	N–H bending	Amide III (Sharma et al. 2020)
1249	N–H in plane bending paired with O=C–N bending and C–N stretching	Amide III (Sharma et al. 2020)
1115	Stretching of glycogen	Glucose (Selvam and Gunasekaran 2018)
1080	CO symmetric stretching	Glucose (Selvam and Gunasekaran 2018)

Detection of disease

To identify differences between the healthy, unhealthy, CVD, diabetic and CVD-diabetic fingernails, five areas of interest were examined and variation between the absorbance levels of each group noted (Figure 1). As the healthy group was classed as the majority and the remaining groups, the minority, data balancing was carried out. Therefore, five participants were selected, one from each group. The fingernail sets matched in completeness (number of fingernail clippings within the set) and number of spectra taken ($n = 30$). An equal balance of spectra per fingernail group, ensured that overfitting of models was avoided and allowed an equal comparison between the groups. Participants included MWS1 (healthy), MWS46 (hypertension), MWS51 (T1DM), MWS57 (T1DM and CAD) and MWS98 (elevated blood pressure). The absorbance levels for the selected regions represented the ATR-FTIR of key endogenous compounds and showed variation between the healthy, unhealthy and diseased fingernails. ATR-FTIR activity was based on the following criteria: number of bands, the range, signal-to-noise ratio and maximum absorption intensity.

The first area of interest was selected between 3570 and 2999 cm^{-1} and was attributed to amide groups and the fingernails' proteins (Selvam and Gunasekaran 2018; Sharma et al. 2020). Within the aforementioned region, unhealthy participant MWS98 demonstrated the highest ATR-FTIR activity and was followed by healthy > CVD-diabetic > diabetic > CVD

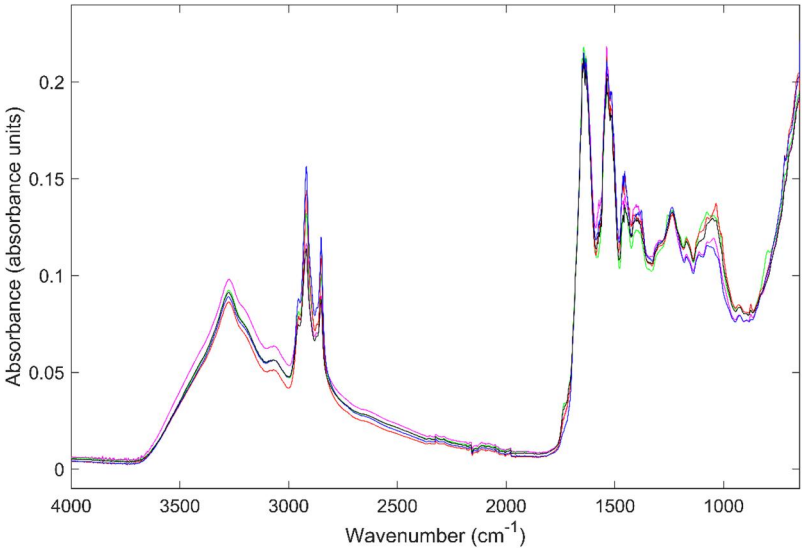

Figure 1. ATR-FTIR spectra of healthy (green), unhealthy (magenta), cardiovascular disease (CVD) (red), diabetic (blue) and CVD-diabetic (black) fingernails.

participants. Previous research made apparent the relationship between high levels of proteins and high blood pressure (Appel 2003). Thus, providing accountability for the increased ATR-FTIR activity of proteins within this region and unhealthy fingernail clippings. The healthy fingernail set demonstrated the second highest ATR-FTIR activity of this area and this could be indicative of the participant's habits of smoking (2–8 cigarettes daily). Despite limited research linking the fingernail's proteins and smoking, previous research demonstrated that cigarette smoking increased inflammation and as a result increased the expression of proteins in plasma (Kolli 2023).Interestingly, participants MWS46, MWS51 and MWS57, did not report any smoking habits and showed the lowest ATR-FTIR activity of proteins.

The second area of interest was located between 3000 and 2828 cm^{-1} and was associated with lipids and cholesterol (Sharma et al. 2020; Sundaram et al. 2016). At this region, diabetic fingernails possessed the highest absorbance and in turn ATR-FTIR activity, followed by CVD > healthy > unhealthy > CVD-diabetic fingernails. As many diabetics suffer from hyperglycemia, the high ATR-FTIR activity of lipids for diabetic fingernails is not unexpected (Verghese et al. 1990). CVD fingernails also showed a strong ATR-FTIR activity within this region, which was also attributed hyperglycemia commonly seen in the development of CVDs. Similarly, between the region 1482–1426 cm^{-1} diabetic fingernails showed the highest ATR-FTIR activity followed by CVD > unhealthy > CVD-diabetic and was attributed to amino acids, lipids and triglycerides. Within the region 1424–1362 cm^{-1}, high ATR-FTIR activity of amino acids was also observed in unhealthy > diabetic > CVD > CVD-diabetic > healthy fingernails. The high ATR-FTIR of amino acids within the fingernails is reflective of circulating amino acid levels found within the plasma. For example, work by Cai et al. (2024) and Fine, Wilkins, and Sawicki (2024) demonstrated that sufferers of CVDs, DM and/or elevated blood pressure showed high levels of amino acids such as isoleucine, leucine and valine.

Therefore, we suggest that the ATR-FTIR activity of key endogenous compounds found in the fingernails is reflective of circulating endogenous compounds within the blood.

Amide I and amide II groups relating to the fingernails' protein structure was detected at 1674–1588 cm^{-1} (Farhan, Sastry, and Mandal 2011; Fernández-Higuero et al. 2014; Gunasekaran et al. 2010; Sundaram et al. 2016). Within this region, healthy participant MWS1 produced the highest ATR-FTIR activity, followed by diabetic > CVD > unhealthy > CVD-diabetic participants. Sihota et al. (2019) investigated the relationship between amide content of healthy control vs. controlled and uncontrolled diabetic cases. This work demonstrated that amides I and II content decreased in both controlled and uncontrolled diabetic cases (Sihota et al. 2019). Thus, indicating that the presence of DM impaired protein regulation and disrupted the keratin structure of the fingernail.

Additional spectral interpretation assessments were carried out using the full spectral dataset ($n = 126$ fingernail sets) and revealed the presence of additional ATR-FTIR bands that were associated to the presence of disease. For example, an additional band was identified at 1115 cm^{-1} (stretching of glycogen) and was attributed to the presence of glucose (Selvam and Gunasekaran 2018). Glucose is deposited into the fingernail in the form of advanced glycation end-products (AGEs) or glycated proteins. Thus, the appearance of glucose within the diabetic fingernail spectra is not unexpected. In fact, several diabetic participants including MWS43, MWS51 and MWS58, demonstrated ATR-FTIR activity at 1115 cm^{-1}. It is worth noting that while the aforementioned band was detected for several non-diabetic participants, the ATR-FTIR activity of this band was lower in non-diabetic participants. For instance, the ATR-FTIR activity of band 1115 cm^{-1} for healthy participant MWS5 was 0.127 absorbance units. Whereas diabetic participant MWS43 possessed 0.150 absorbance units at the band of interest. Thus, demonstrating an accumulation of glucose within diabetic fingernails. In like fashion, a band located at 1080 cm^{-1} (CO symmetric stretching) was also indicative of glucose (Selvam and Gunasekaran 2018). Similarly diabetic participants showed a greater ATR-FTIR activity at this band than healthy participants (0.116 vs.0.0987 absorbance units).

For several ATR-FTIR spectra, the absence of band 1738 cm^{-1} was noticeable. The aforementioned band lends itself to high-density lipoproteins (HDLs) and can be attributed to C=O groups of cholesterol esters (Barton 2004; Selvam and Gunasekaran 2018). The presence of band 1738 cm^{-1} was noted for a low number of participants ($n = 26$), who were classified as healthy ($n = 20$), unhealthy ($n = 2$), CVD ($n = 2$) and diabetic ($n = 2$). HDLs, often referred to as 'good cholesterol', play an imperative role in lipid metabolism and have previously demonstrated a protective effect against CVDs (Farhan, Sastry, and Mandal 2011). Through the transportation of cholesterol from peripheral tissues such as arterial walls to the liver for excretion, HDLs prevent the build-up of cholesterol in blood vessels; thus, reducing CVD risk (Das and Ingole 2023). Hausenloy and Yellon (2008) also made apparent their anti-inflammatory, antioxidant and anti-thrombotic benefits, which further contribute to their cardioprotective properties. Therefore, a low level of HDLs is considered a risk factor for CVDs (Das and Ingole 2023).

Hypoalphalipoproteinemia, where HDL levels are < 40 and < 50 mg/dL in males and women, respectively, is often the consequence of poor lifestyle choices including a lack

of exercise, unhealthy diets and extreme alcohol consumption (Das and Ingole 2023; Schaefer et al. 2016). Moreover, have also been associated with insulin resistance, DM and other medical conditions such as cancer (Penson et al. 2019). This was the case for participant MWS15, who had previously been diagnosed with breast cancer, and a number of CVD, diabetic and CVD-diabetic participants, who did not present ATR-FTIR activity at band 1738 cm^{-1}. In cases where HDLs were absent in healthy spectra, the clinical data was referred to and revealed that participants made poor lifestyle choices including infrequent or no exercise, frequent fast-food consumption, unbalanced diet and smoking.

Between the region 1582–1562 cm^{-1}, the presence of homocysteine was detected and was attributed to NH_2 scissoring (Assi et al. 2019). Hyperhomocysteinemia, elevated levels of homocysteine, creates blood vessel irritation and in severe cases hardening of arteries (atherosclerosis) and blood clots (venous thrombosis) (Varga et al. 2005). Several of the CVD participants, including MWS46, MWS47, MWS52, MWS56 and MWS71, demonstrated high ATR-FTIR activity within this region. Increased activity of homocysteine has also been associated with lifestyle factors including consumption of alcohol and caffeine, folate intake, smoking and physical exercise (Bree et al. 2001; Giles et al. 1999; Maron and Loscalzo 2007; Nygård et al. 1997, 1998; Selhub et al. 1993; Ubbink et al. 1998; Vollset et al. 2001). The aforementioned factors were reported by several participants including MWS32, MWS54, MWS61–MWS63, MWS89, MWS90, MWS99, MWS100 and MWS101, who presented ATR-FTIR activity within $1582 - 1562\ cm^{-1}$.

Application to machine learning algorithms

To further understand the relationship between disease and the fingernails' endogenous compounds, several MLAs were applied. The first applied MLA was CWS, which demonstrated the relationship or correlation between fingernails of similar or dissimilar characteristics/disease status. As 30 spectra were taken per fingernail set, 150 spectra (five sets of clippings) were applied to the model and prevented this issue of overfitting or creating an overly complex model. As highlighted by Figure 2, each fingernail set produced an r value of +1 against itself, indicating a positive match. Five spectra, taken from fingernail set MWS1, produced r values of +1 against one another and indicated a match. Moreover, a minimal number of mismatches ($n = 3$) were seen between healthy vs. healthy spectra. Thus, ATR-FTIR was able to detect healthy fingernails. When compared to unhealthy and diseased fingernails, several mismatches were observed. For example, when healthy spectra were correlated against unhealthy spectra, 53 mismatches were identified. Healthy spectra vs. CVD, diabetic and CVD-diabetic spectra produced 71, 119 and 10 mismatches, respectively. Thus, across the four remaining groups, ATR-FTIR showed the greatest discrimination between healthy vs. diabetic fingernails.

A total of 386 mismatches were detected for unhealthy spectra. The largest number of mismatches was observed between unhealthy vs. diabetic spectra with a total of 146 mismatches. Unhealthy vs. CVD spectra also produced a high number of mismatches ($n = 107$), followed by unhealthy vs. healthy spectra, which showed 71 mismatches. Several type II errors were identified, as 28 unhealthy spectra mismatched against

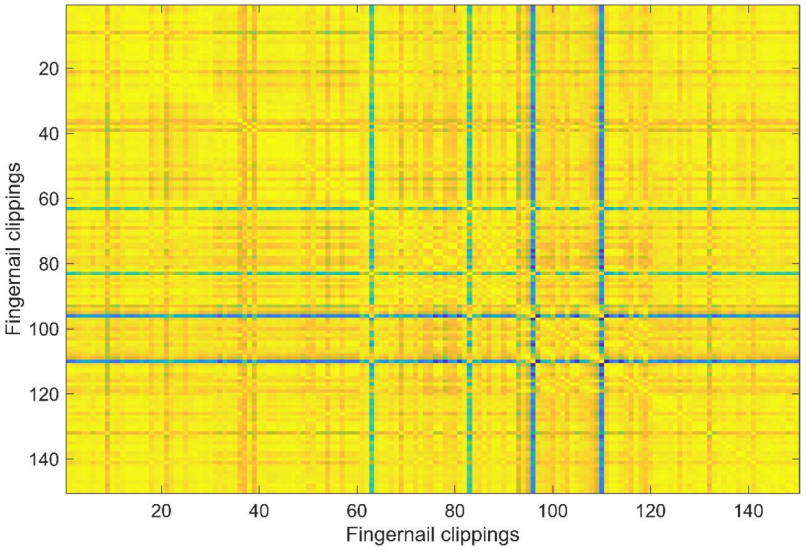

Figure 2. Correlation in wavenumber space (CWS) of average ATR-FTIR spectra taken from healthy (1–30), unhealthy (31–60), CVD (61–90), diabetic (91–120) and CVD-diabetic (121–150) fingernails measured using the Agilent 4500a ATR-FTIR spectrometer equipped with an ATR diamond. The color bar demonstrated the correlation between the spectra and made apparent the corresponding r-value. Dark blue represented a minimum r value of 0.75, while the bright yellow demonstrated the maximum r value of 0.9999. Between the minimum and maximum r values, a blue color corresponded to an r value of 0.80–0.85, light blue corresponded to an r value of 0.85–0.90, green/yellow corresponded to an r value of 0.90–0.95 and orange/yellow corresponded to an r value of 0.95–1.00.

spectra of the same unhealthy status. Nevertheless, ATR-FTIR spectroscopy paired with CWS demonstrated the ability to differentiate between unhealthy and healthy or disease spectra.

Overall, CVD spectra produced 523 mismatches across the five groups. Despite CVD and DM sharing similar pathophysiological features, the highest number of mismatches ($n = 160$) was recorded for the aforementioned groups (De Rosa et al. 2018). A high number of mismatches were also observed between CVD and unhealthy fingernails ($n = 107$). The ATR-FTIR spectroscopy paired with CWS, also showed some ability to differentiate between CVD and healthy spectra, with 70 mismatches between the two groups. Nonetheless, 121 mismatches were noted between CVD vs. CVD spectra and was attributed to type II error.

Across the five groups, diabetic spectra demonstrated the highest number of mismatches ($n = 766$). In like manner to the classification of CVD spectra, diabetic vs. CVD spectra produced the highest number of mismatches ($n = 157$), followed closely by diabetic vs. unhealthy spectra with 147 mismatches, while diabetic vs. healthy spectra produced 120 mismatches. When compared to spectra of the same disease status, a high number of mismatches were observed ($n = 214$). However, it is important to note that while many type II errors were seen, several diabetic spectra ($n = 15$) produced a perfect r value of +1 against other diabetic spectra.

The lowest number of mismatches was observed for the correlation of CVD-diabetic spectra, which produced a total of 260 mismatches. Against the remaining five groups,

CVD-diabetic fingernails produced 11 (healthy), 45 (unhealthy), 65 (CVD) and 129 (diabetic) mismatches. Against spectra of the same disease status, a minimal number ($n = 10$) of mismatches were identified. However, it is worth noting that the limited number of mismatches between CVD-diabetic spectra and the remaining four groups can be attributed to the CVD-diabetic participant sharing similar CVD (CAD) and diabetic (T1DM) diagnoses as the CVD and diabetic participants, MWS46 and MWS51, respectively.

Across the CWS model, 2191 mismatches were identified and demonstrated the ability of ATR-FTIR spectroscopy paired with CWS to differentiate between fingernails of different health or disease status. In addition, ATR-FTIR spectroscopy correctly correlated spectra with the same health or disease status, particularly healthy spectra, which only produced three type II errors. The presence of several mismatches between fingernail spectra of differing health or disease (type I error) can be attributed to the sharing of the same set of endogenous compounds across all fingernails, despite the absence or presence of disease. Therefore, while disease such as CVDs and/or DM did alter the circulation of key endogenous compounds, the presence of disease did not significantly alter the ATR-FTIR spectra. Hence indicating that for the detection of disease, in-depth spectral interpretation of key IR bands and absorbance levels are necessary.

A PCA model was then applied to fingernail spectra for the visualization of clusters and patterns within the spectral data. The PCA model demonstrated a high variance of 98.9%, with PC1 corresponding to 98.1% of the variance and PC2 to 0.818% of the variance. Figure 3 demonstrated the clustering of the five groups and confirmed shared epidemiological and biological mechanisms of CVDs and DM. For example, hyperglycemia, a common diabetic symptom, is also extremely prevalent in patients with CVDs (Diabetes UK 2024). High blood sugar levels have associated with blood vessel damage and as a result increases inflammation and disrupts normal blood flow.

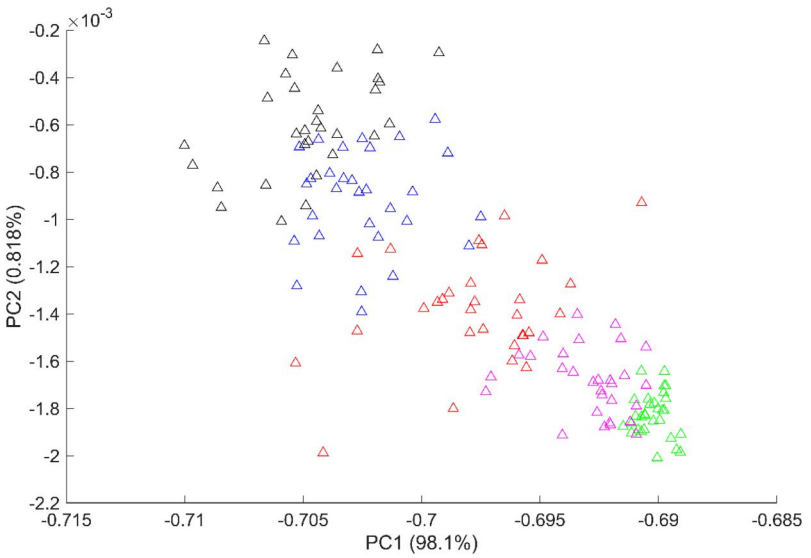

Figure 3. Principal component analysis (PCA) of ATR-FTIR spectra of healthy (green), unhealthy (magenta), CVD (red), diabetic (blue) and CVD-diabetic (black) fingernails.

In extreme cases, whereby the two conditions occur as comorbidities, microvascular and macrovascular complications worsen (Kotis et al. 2005). Similarly, CVD-diabetic and diabetic spectra were clustered together based on their shared diagnosis of T1DM. Thus, shared similar ATR-FTIR activity of key endogenous compounds. In like manner, CVD and unhealthy spectra were presented in close proximity, which can be attributed to the similarities seen between hypertension (>130 mm Hg) and elevated blood pressure (120–129 mm Hg) (World Health Organisation 2023). Through the poor management of elevated blood pressure, hypertension can occur, causing further narrowing and damage to the arteries and preventing sufficient blood flow (World Health Organisation 2023). Thus, the deposition of endogenous compounds and corresponding ATR-FTIR activity seen with the fingernails of participants with high blood pressure or hypertension is likely to be similar.

SOMs were applied as an additional proof of concept and validated PCA findings. The SOMs of choice included neighbor weight distances (Figure 4) and sample hits (Figure 5). Neighbor weight distances made apparent the distances and relationships between the inputted spectra. Dark colors including black, dark red and red represented smaller distances between neurons and in term highlighted close relationships between the inputted spectra. For instance, two neurons connected by the black hexagon correspond to healthy and unhealthy spectra. Therefore, confirming the close clustering of healthy and unhealthy spectra within the previous PCA model. Despite the presence of high blood pressure, the ATR-FTIR activity of key endogenous compounds was not significantly altered which can be attributed to the management of the condition. Participant MWS98 reported the use of Aldomet (methyldopa), which is administered

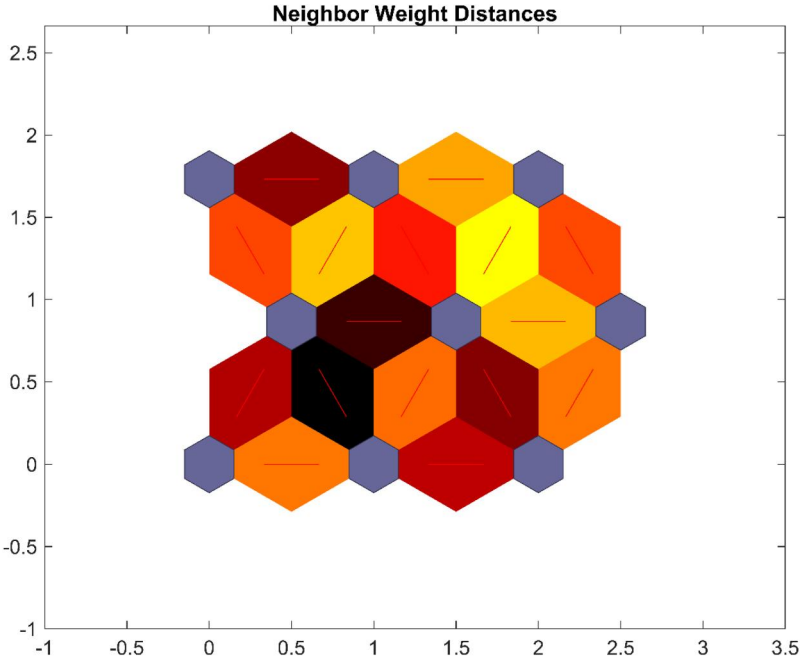

Figure 4. Self-organizing map (SOM) neighbor weight distances of ATR-FTIR spectra of healthy, unhealthy, CVD, diabetic and CVD-diabetic fingernails.

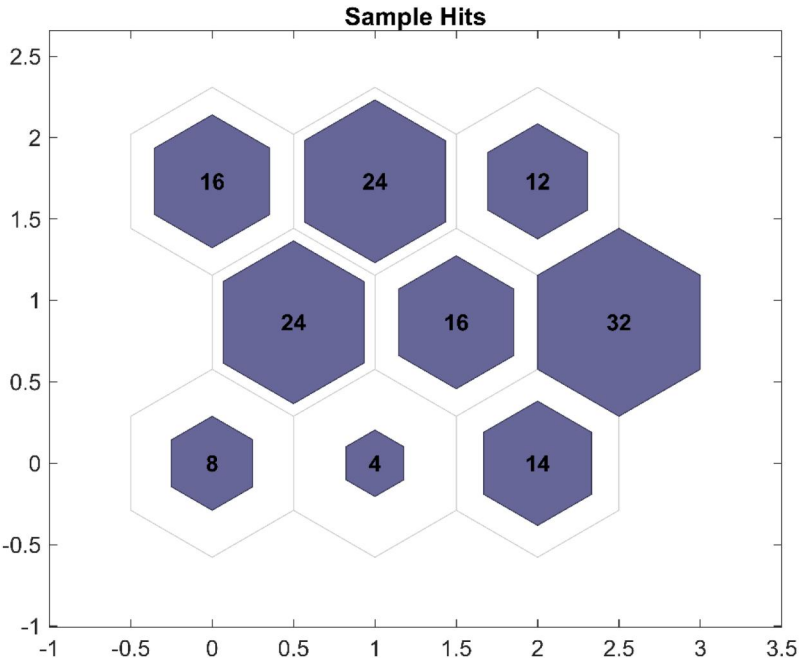

Figure 5. SOM sample hits of ATR-FTIR spectra of healthy, unhealthy, CVD, diabetic and CVD-diabetic fingernails.

for the treatment of high blood pressure. Through the repeated use of such prescription drugs, it is likely that participant MWS98 has managed their condition well and prevented severe damage to the arteries. Therefore, allowing endogenous compounds to move freely to finger's palmer digital arteries and to carry out passive diffusion into the fingernail. Light colored hexagons such as orange, yellow and light yellow were indicative of larger distances and loosely related spectra.

For example, a light yellow hexagon was seen between the neurons representing the healthy and CVD-diabetic fingernail sets and further confirmed previous PCA findings. The high variability between healthy vs. CVD-diabetic fingernails can be attributed to the diagnosis of CAD and T1DM. CAD is characterized by the development of plaque (fatty deposits) within artery passages. The formation of such fatty deposits decreases the supply of blood and oxygen, as well as the distribution of vital nutrients around the body (Pandey et al. 2020). Thus, the passive diffusion of endogenous compounds for participant MWS57 was limited. The presence of T1DM is also detrimental to the passage of nutrient and endogenous compounds around the body and to tissues such as fingernails. Hyperglycemia can not only cause blood vessel damage but can also block the passage of nutrients (Diabetes UK 2024). Therefore, the high variability seen between the healthy fingernails, with normal circulation, and CVD-diabetic fingernails, is not unexpected.

Samples hits were also explored to further confirm the grouping of fingernails based on their ATR-FTIR activity. Within the model, a total of nine groups were accounted for and confirmed the relationships identified within the PCA model. In particular, the relationship between CVD and diabetic fingernails, as well as the relationship between CVD and unhealthy clippings. Group one ($n = 16$) corresponded to spectra taken from

CVD-diabetic fingernails. Group two ($n = 24$) showed a crossover between CVD and CVD-diabetic spectra. A crossover was also demonstrated between CVD and diabetic fingernails in groups three ($n = 12$) and four ($n = 24$). Group five consisted solely to spectra taken from CVD fingernails. Group five ($n = 16$). Group six ($n = 32$) corresponded to CVD, unhealthy and healthy spectra. Finally, groups seven ($n = 8$), eight ($n = 4$) and nine ($n = 14$) represent unhealthy and healthy spectra.

Conclusions

This study demonstrated the feasibility of ATR-FTIR spectroscopy and MLAs for the detection of CVDs and/or DM in fingernails. Spectral interpretation allowed for identification of key ATR-FTIR bands, as well as their corresponding functional groups and related endogenous compounds. The detection of these compounds, such as amino acids, lipids and proteins, demonstrated the fingernail's structural integrity and keratin quality. Additional disease-related compounds such as glucose, HDLs and homocysteine were also identified. Specifically, the presence of glucose indicated DM, while homocysteine demonstrated the presence of CVDs such as atherosclerosis and hypertension. In cases where low ATR-FTIR activity of HDLs were observed, CVD risk was common. Nonetheless, low ATR-FTIR activity of HDLs was also attributed to poor lifestyle choices such as a lack of exercise, poor diet and smoking.

Six areas of interest were investigated and provided key information regarding the ATR-FTIR activity of endogenous compounds and their deposition into healthy and unhealthy/diseased fingernails. It was demonstrated that increased ATR-FTIR activity of amide I and the fingernail's protein was associated with high blood pressure and smoking. Moreover, high ATR-FTIR activity of lipids and cholesterol were primarily observed in diabetic clippings. The application of MLAs further confirmed the successful application of ATR-FTIR spectroscopy for the detection of CVDs and/or DM in fingernails.

Firstly, the CWS model demonstrated a high number of mismatches between spectra of varying health/disease status. Thus, ATR-FTIR paired with CWS can efficiently match or mismatch the spectra based on similar or dissimilar spectral characteristics created by disease and lifestyle. The application of a PCA model, further confirmed this finding and grouped fingernail spectra based on their health/disease status. While some crossover was observed between the five groups of interest, interaction was minimal and when encountered, confirmed the presence of similar epidemiological and biological mechanisms between CVDs and DM, as well as high blood pressure and hypertension. Crossover was also apparent in the utilized SOMs (neighbor weight distances and samples hits), which highlighted relationships between CVD and diabetic clippings, CV and unhealthy clippings and finally CVD, diabetic and CVD-diabetic clippings.

To conclude, the Agilent ATR-FTIR spectrometer offered noninvasive and non-intrusive analysis of fingernails, which can be applied in LMICs. Its ability to detect-related compounds including glucose, HDLs and homocysteine makes apparent the feasibility of ATR-FTIR as a novel disease detection tool that in future years may replace traditional detection techniques such as blood work and CT scans, which are expensive, invasive and intrusive.

Ethical considerations

Ethical approval for the completion of this work was provided by two institutes: Liverpool John Moores University (23/PBS/009A) in the UK and the Lebanese University (2022-0104) in Lebanon.

Consent to participate

Informed consent to participate was provided by participants in the form of a signed consent form.

Consent for publication

Participants were made aware of the publication of data and their identities have been anonymized for their protection. Participants provided informed consent *via* a signed consent form.

Disclosure statement

No potential conflict of interest was reported by the authors.

Funding

The authors received no financial support for the research, authorship and/or publication of this article.

Data availability statement

The datasets generated during and/or analyzed during the current study can be accessed upon request from eSystems Engineering Society: https://dese.ai/medicaldatabank-viewdata/.

References

Abid, A., M. J. Zhang, V. K. Bagaria, and J. Zou. 2018. Exploring patterns enriched in a dataset with contrastive principal component analysis. *Nature Communications* 9 (1):2134. doi:10.1038/s41467-018-04608-8.

Al Hamid, A. M. 2015. Medicine related hospitalisation in the UK and Saudi Arabia of adults with cardiovascular disease and/or diabetes, 82–3. Hatfield, UK: University of Hertfordshire.

Al Hamid, A., R. Beckett, M. Wilson, Z. Jalal, E. Cheema, D. Al-Jumeily Obe, T. Coombs, K. Ralebitso-Senior, and S. Assi. 2024. Gender bias in diagnosis, prevention, and treatment of cardiovascular diseases: A systematic review. *Cureus* 16 (2):e54264. doi:10.7759/cureus.54264.

Alajaji, S. A., R. Sabzian, Y. Wang, A. S. Sultan, and R. Wang. 2025. Learning methods for head and neck precancer and cancer diagnosis and prognosis. *Cancers* 17 (5):796. doi:10.3390/cancers17050796.

American Diabetes Association. 2008. Economic costs of diabetes in the U.S. in 2007. *Diabetes Care* 31 (3):596–615. doi:10.2337/dc08-9017.

American Diabetes Association. 2011. Diagnosis and classification of diabetes mellitus. *Diabetes Care* 34 (Suppl 1):S62–S69. doi:10.2337/dc11-S062.

Amini, K., A. Mirzaei, M. Hosseini, H. Zandian, I. Azizpour, and Y. Haghi. 2022. Assessment of electrocardiogram interpretation competency among healthcare professionals and students of Ardabil University of Medical Sciences: A multidisciplinary study. *BMC Medical Education* 22 (1):448. doi:10.1186/s12909-022-03518-0.

Appel, L. J. 2003. The effects of protein intake on blood pressure and cardiovascular disease. *Current Opinion in Lipidology* 14 (1):55–9. doi:10.1097/00041433-200302000-00010.

Assi, S., I. Abbas, B. Arafat, K. Evans, and D. Al-Jumeily. 2023. Authentication of Covid-19 vaccines using synchronous fluorescence spectroscopy. *Journal of Fluorescence* 33 (3):1165–74. doi:10.1007/s10895-022-03136-5.

Assi, S., I. Robertson, T. Coombs, J. McEachran, and K. Evans. 2019. The use of portable near-infrared spectroscopy for authenticating cardiovascular medicines. *Spectroscopy* 34:46–54.

Bahia, L. R., D. V. Araujo, B. D. Schaan, S. A. Dib, C. A. Negrato, M. P. Leão, A. J. Ramos, A. C. Forti, M. B. Gomes, M. C. Foss, et al. 2011. The costs of type 2 diabetes mellitus outpatient care in the Brazilian public health system. *Value in Health* 14 (5 Suppl 1):S137–S140. doi:10.1016/j.jval.2011.05.009.

Bangalore, S., G. W. Barsness, G. D. Dangas, M. J. Kern, S. V. Rao, L. Shore-Lesserson, and J. E. Tamis-Holland. 2021. Evidence-based practices in the cardiac catheterisation laboratory: A scientific statement from the american heart association. *Circulation* 144 (5):e107–19. doi:10.1161/CIR.0000000000000996.

Bantignies, J. L., G. Fuchs, G. L. Carr, G. P. Williams, D. Lutz, and S. Marull. 1998. Organic reagent interaction with hair spatially characterised by infrared microspectroscopy using synchrotron radiation. *International Journal of Cosmetic Science* 20 (6):381–94. doi:10.1046/j.1467-2494.1998.177055.x.

Barton, P. A. 2004. Forensic taphonomy investigation of single α – keratin fibres under environmental stress using a novel application of FTIR-ATR spectroscopy and chemometrics. PhD thesis, Queensland University of Technology, Brisbane City, Australia.

Bree, A., W. M. Verschuren, H. J. Blom, and D. Kromhout. 2001. Association between B vitamin intake and plasma homocysteine concentration in the general dutch population aged 20–65 y. *AJCN* 73:1027–33.

Cai, S., Y. Fu, J. Chen, M. Tian, and X. Li. 2024. Casual relationship between branched-chain amino acids and hypertension: A Mendelian randomisation study. *JAHA* 13:e032084.

Camargo, A. 2022. PCAtest: Testing the statistical significance of principal component analysis in R. *PeerJ*. 10:e12967. doi:10.7717/peerj.12967.

Coopman, R., T. Van de Vyver, A. S. Kishabongo, P. Katchunga, E. H. Van Aken, J. Cikomola, T. Monteyne, M. M. Speeckaert, and J. R. Delanghe. 2017. Glycation in human fingernail clippings using ATR-FTIR spectrometry, A new marker for the diagnosis and monitoring of diabetes mellitus. *Clinical Biochemistry* 50 (1–2):62–7. doi:10.1016/j.clinbiochem.2016.09.001.

Das, P., and N. Ingole. 2023. Lipoproteins and their effects on the cardiovascular system. *Cureus* 15 (11):e48865. doi:10.7759/cureus.48865.

De Rosa, S., B. Arcidiacono, E. Chiefari, A. Brunetti, C. Indolfi, and D. P. Foti. 2018. Type 2 diabetes mellitus and cardiovascular disease: Genetic and epigenetic links. *Frontiers in Endocrinology* 9:1–13. doi:10.3389/fendo.2018.00002.

Dedefo, M., H. Mwambi, S. Fanta, and N. Assefa. 2018. Spatiotemporal mapping and detection of mortality cluster due to cardiovascular disease with Bayesian hierarchical framework using integrated nested Laplace approximation: A discussion of suitable statistics applications in Kersa, Oromia, Ethiopia. *Geospatial Health* 13 (2):1–9. doi:10.4081/gh.2018.681.

Diabetes UK. 2024. Diabetes and heart disease. Accessed September 2, 2024. https://www.diabetes.org.uk/guide-to-diabetes/complications/cardiovascular_disease#:~:text=If%20you%20have%20high%20blood,builds%20up%20in%20your%20blood.

Fadlelmoula, A., S. O. Catarino, G. Minas, and V. Carvalho. 2023. A review of machine learning methods recently applied to FTIR spectroscopy data for the analysis of human blood cells. *Micromachines* 14 (6):1145. doi:10.3390/mi14061145.

Farhan, K. M., T. P. Sastry, and A. B. Mandal. 2011. Comparative study on secondary structural change in diabetes and non-diabetic human fingernail nail specimen by using FTIR spectra. *Clinica Chimica Acta* 412:386–9.

Fernández-Higuero, J., A. M. Salvador, C. Martín, J. C. G. Milicua, and L. R. Arrondo. 2014. Human LDL structural diversity studies by IR spectroscopy. *PLoS One* 9 (3):e92426. doi:10.1371/journal.pone.0092426.

Fine, K. S., J. T. Wilkins, and K. T. Sawicki. 2024. Circulating branched chain amino acids and cardiometabolic disease. *Journal of the American Heart Association* 13 (7):e031617. doi:10.1161/JAHA.123.031617.

Gandhi, T. K., A. Kachalia, E. J. Thomas, A. L. Puopolo, C. Yoon, T. A. Brennan, and D. M. Studdert. 2006. Missed and delayed diagnoses in the ambulatory setting: A study of closed malpractice claims. *Annals of Internal Medicine* 145 (7):488–96. doi:10.7326/0003-4819-145-7-200610030-00006.

Ghazali, S. M., Z. Seman, K. C. Cheong, L. K. Hock, M. Manickam, L. K. Kuay, A. F. Yusoff, F. I. Mustafa, and A. N. Mustafa. 2015. Sociodemographic factors associated with multiple cardiovascular risk factors among Malaysian adults. *BMC Public Health* 15 (1):68. doi:10.1186/s12889-015-1432-z.

Giles, W. H., S. J. Kittner, J. B. Croft, M. A. Wozniak, R. J. Wityk, B. J. Stern, M. A. Sloan, T. R. Price, R. H. McCarter, R. F. Macko, et al. 1999. Distribution and correlates of elevated total homocyst(e)ine: The stroke prevention in young women study. *Annals of Epidemiology* 9 (5):307–13. doi:10.1016/s1047-2797(99)00006-x.

Gillam, L. D., and L. Marcoff. 2024. Echocardiography: Past, present and future. *Circulation: JACC Cardiovascular Imaging* 17:e016517.

Gunasekaran, S., A. Bright, T. S. R. Devi, R. Arunbalaji, G. Anaand, J. Dhanalaksmi, and S. Kumaresan. 2010. 2010. Experimental and semi-empirical computations of the vibrational spectra of methionine, homocysteine and cysteine. *Archives of Physics Research* 1:12–26.

Hausenloy, D. J., and D. M. Yellon. 2008. Targeting residual cardiovascular risk: Raising high-density lipoprotein cholesterol levels. *Postgraduate Medical Journal* 84 (997):590–8. doi:10.1136/hrt.2007.125401.

Jee, R. 2024. Infrared spectroscopy. In *Clarke's analysis of drugs and poisons*, ed. A. C. Moffat, A. C. Osselton, and S. P. Elliot. London, UK: Pharmaceutical Press.

Jolliffe, I., and J. Cadima. 2016. Principal component analysis: A review and recent developments. *Philosophical Transactions of the Royal Society A: Mathematical, Physical and Engineering Sciences* 374:1–4.

Kazemi, Z., K. Hajimiri, F. Saghatchi, M. Molazadeh, and H. Rezaeejam. 2023. Assessment of the Knowledge Level of Radiographers and CT Technologists Regarding Computed Tomography Parameters in Iran. *Radiation Medicine and Protection* 4 (1):60–4. doi:10.1016/j.radmp.2023.01.002.

Kolli, A. R. 2023. Plasma protein binding and tissue retention kinetics influence the rate and extend of nicotine delivery to the brain. *Toxicology Letters* 380:69–74. doi:10.1016/j.toxlet.2023.04.006.

Kotis, J. B., A. C. Wilson, R. S. Freudenberger, N. M. Cosgrove, S. L. Pressel, and B. R. Davis. 2005. Long-term Effect of diuretic-based therapy on fatal outcomes in subjects with isolated systolic hypertension with and without diabetes. *AJC* 95:29–35.

Kumar, S., A. Srinivasan, and F. Nikolajeff. 2018. Role of infrared spectroscopy and imaging in cancer diagnosis. *Current Medicinal Chemistry* 25 (9):1055–72. doi:10.2174/0929867324666170523121314.

Ladapo, J. A., S. Blecker, and P. S. Douglas. 2010. Physician decision-making and trends in use of cardiac stress testing to diagnose coronary heart disease in the United States, 1993. *Annals of Internal Medicine* 161:482–90. doi:10.7326/M14-0296.

Leon, B. M., and T. M. Maddox. 2015. Diabetes and cardiovascular disease: Epidemiology, biological mechanisms, treatment recommendations and future research. *World Journal of Diabetes* 6 (13):1246–58. doi:10.4239/wjd.v6.i13.1246.

Lopez-Mattei, J., E. H. Yang, L. A. Baldassarre, A. Agha, R. Blankstein, A. D. Choi, M. Y. Chen, N. Meyersohn, R. Daly, A. Slim, et al. 2023. Cardiac computed tomographic imaging in cardio-

oncology: An expert consensus document of the society of cardiovascular computed tomography (SCCT). *JCCT* 17:66–83.
Lusignan, S., K. Khunti, J. Belsey, A. Hattersley, J. Vlymen, H. Gallagher, C. Millett, H. J. Hague, C. Tomson, K. Harris, et al. 2010. A method of identifying and correcting miscoding, misclassification and misdiagnosis in diabetes: A pilot and validation study of routinely collected data. *Diabetic Medicine* 27 (2):203–9. doi:10.1111/j.1464-5491.2009.02917.x.
Lusignan, S., N. Sadek, H. Mulnier, A. Tahir, D. Russel-Jones, and K. Khunti. 2011. Miscoding, misclassification and misdiagnosis of diabetes in primary care. *Diabetic Medicine* 29:181–9.
Maiti, K. S. 2023. Non-invasive disease specific biomarker detection using infrared spectroscopy: A review. *Molecules* 28 (5):2320. doi:10.3390/molecules28052320.
Maron, B. A., and J. Loscalzo. 2007. Should hyperhomocysteinemia be treated in patients with atherosclerotic disease? *Current Atherosclerosis Reports* 9 (5):375–83. doi:10.1007/s11883-007-0048-x.
Matheus, A. S., L. R. Tannus, R. A. Cobas, C. C. Palma, C. A. Negrato, and M. B. Gomes. 2013. Impact of diabetes on cardiovascular disease: An update. *International Journal of Hypertension* 2013:653789. doi:10.1155/2013/653789.
Mitu, B., M. Cerda, R. Hrib, V. Trojan, and L. Halámková. 2023. Attenuated total reflection fourier transform infrared spectroscopy for forensic screening of long-term alcohol consumption from human nails. *ACS Omega* 8 (24):22203–10. doi:10.1021/acsomega.3c02579.
Nygård, O., H. Refsum, P. M. Ueland, and S. E. Vollset. 1998. Major lifestyle determinants of plasma total homocysteine study. *AJCN* 67:263–70.
Nygård, O., H. Refsum, P. M. Ueland, I. Stensvold, J. E. Nordrehaug, G. Kvåle, and S. E. Vollset. 1997. Coffee consumption and plasma total homocysteine: The hordaland homocysteine study. *The American Journal of Clinical Nutrition* 65 (1):136–43. doi:10.1093/ajcn/65.1.136.
Pandey, R., M. Kumar, J. Majdoubi, M. Rahimi-Gorji, and V. K. Srivastav. 2020. A review study on blood in human coronary artery: Numerical approach. *Computer Methods and Programs in Biomedicine* 187:105243. doi:10.1016/j.cmpb.2019.105243.
Panju, A. A., B. R. Hemmelgarn, G. H. Guyatt, and D. L. Simel. 1998. Is this patient having a myocardial infarction? *JAMA* 280 (14):1256–63. doi:10.1001/jama.280.14.1256.
Penson, P., D. L. Long, G. Howard, V. J. Howard, S. R. Jones, S. S. Martin, D. P. Mikhailidis, P. Muntner, M. Rizzo, D. J. Rader, et al. 2019. Associations between cardiovascular disease, cancer and very low high-density lipoprotein cholesterol in reasons for geographical and racial differences in stroke (REGARDS) study. *Cardiovascular Research* 115 (1):204–12. doi:10.1093/cvr/cvy198.
Phillips, R. L., Jr., L. A. Bartholomew, S. M. Dovey, G. E. Fryer, Jr., T. J. Miyoshi, and L. A. Green. 2004. Learning from malpractice claims about negligent, adverse events in primary care in the United States. *BMJ Quality and Safety* 1:121–6. doi:10.1136/qshc.2003.008029.
Quinn, G. R., D. Ranum, E. Song, M. Linets, C. Keohane, H. Riah, and P. Greenberg. 2017. Missed diagnosis of cardiovascular disease in outpatient general medicine: Insights from malpractice. *JQPS* 43:508–16.
Roman, W. P., H. D. Martin, and E. Sauli. 2019. Cardiovascular diseases in Tanzania: The burden of modifiable and intermediate risk factors. *Journal of Xiangya Medicine* 4:33. doi:10.21037/jxym.2019.07.03.
Schaefer, E. J., P. Anthanont, M. R. Diffenderfer, E. Polisecki, and B. F. Asztalos. 2016. Diagnosis and treatment of high density lipoprotein deficiency. *Progress in Cardiovascular Diseases* 59 (2):97–106. doi:10.1016/j.pcad.2016.08.006.
Schiff, G. D., A. L. Puopolo, A. Huben-Kearney, W. Yu, C. Keohane, P. McDonough, B. R. Ellis, D. W. Bates, and Biodolillo, M. 2013. Primary care closed claims experience of massachusetts malpractice insurers. *JAMA Internal Medicine* 173 (22):2063–8. doi:10.1001/jamainternmed.2013.11070.
Selhub, J., P. F. Jacques, P. W. Wilson, D. Rush, and I. H. Rosenberg. 1993. Vitamin status and intake as primary determinants of homocysteinemia in an elderly population. *JAMA* 270 (22):2693–8. doi:10.1001/jama.1993.03510220049033.

Selvam, J. P., and S. Gunasekaran. 2018. Biological analysis of fingernails of healthy and thyroid disordered subjects by FTIR-ATR spectroscopic technique. *International Journal of PharmTech Research* 11 (3):242–52. doi:10.20902/IJPTR.2018.11306.

Sequist, T. D., R. Marshall, S. Lampert, E. J. Buechler, and T. H. Lee. 2006. Missed opportunities in the primary care management of early acute ischemic heart disease. *Archives of Internal Medicine* 166 (20):2237–43. doi:10.1001/archinte.166.20.2237.

Sequist, T. D., S. M. Morong, A. Marston, C. A. Keohane, E. F. Cook, E. J. Orav, and T. H. Lee. 2012. Electronic risk alerts to improve primary care management of chest pain: A randomised controlled trial. *Journal of General Internal Medicine* 27 (4):438–44. doi:10.1007/s11606-011-1911-6.

Sharma, A., S. Mittal, R. Aggarwal, and M. K. Chauhan. 2020. Diabetes and cardiovascular disease: Inter-relation of risk factors and treatment. *Future Journal of Pharmaceutical Sciences* 6 (1):130. doi:10.1186/s43094-020-00151-w.

Sianga, B. E., M. C. Mbago, and A. S. Msengwa. 2025. Predicting the prevalence of cardiovascular diseases using machine learning algorithms. *Intelligence-Based Medicine* 11:100199. doi:10.1016/j.ibmed.2025.100199.

Sihota, P., R. N. Yadav, V. Dhiman, S. K. Bhadada, V. Mehandia, and N. Kumar. 2019. Investigation of diabetic patient's fingernail quality to monitor type 2 diabetes induced tissue damage. *Scientific Reports* 9 (1):3193. doi:10.1038/s41598-019-39951-3.

Silva, S. M. S. D., C. L. Ferreira, J. M. B. Rizzato, G. S. Toledo, M. Furukawa, E. S. Rovai, M. S. Nogueira, and L. F. C. S. Carvalho. 2024. Infrared spectroscopy for fast screening of diabetes and periodontitis. *PD-PDT* 46:104106.

Sundaram, K., S. Gunasekaran, E. Sailatha, P. K. Marthandam, and P. Kuppuraj. 2016. FTIR-ATR spectroscopic technique on human hair fibre—A case study of thyroid patients. *IJASTEMS* 2: 2454–356.

Thompson, B. S., and C. W. Yancy. 2004. Immediate vs delayed diagnosis of heart failurer: Is there a difference in outcomes? Results of a Harris interactive patient survey. *Journal of Cardiac Failure* 10 (4):S125. 2004doi:10.1016/j.cardfail.2004.06.399.

Ubbink, J. B., A. M. Fehily, J. Pickering, P. C. Elwood, and Vermaak, W. J. 1998. 1998. Homocysteine and ischaemic heart disease in the caerphilly cohort. *Atherosclerosis* 140 (2):349–56. doi:10.1016/S0021-9150(98)00139-7.

Vaduganathan, M., G. A. Mensah, J. V. Turco, V. Fuster, and G. A. Roth. 2022. The global burden of cardiovascular diseases and risk: A compass for future health. *Journal of the American College of Cardiology* 80:2361–71.

Varga, E. A., A. C. Sturm, C. P. Misita, and S. Moll. 2005. Homocysteine and MTHFR mutations: Relation to thrombosis and coronary artery disease. *Circulation* 111:e289–93.

Verghese, A., G. Krish, D. Howe, and M. Stonecipher. 1990. The harlequin nail: A marker for smoking cessation. *Chest* 97 (1):236–8. doi:10.1378/chest.97.1.236.

Vollset, S. E., H. Refsum, A. Tverdal, O. Nygård, J. E. Nordrehaug, G. S. Tell, and P. M. Ueland. 2001. Plasma total homocysteine and cardiovascular and noncardiovascular mortality: The hordaland homocysteine study. *AJCN* 74:130–6. doi:10.1093/ajcn/74.1.130.

World Health Organisation. 2019. Cardiovascular diseases. https://www.who.int/news-room/fact-sheets/detail/cardiovascular-diseases-(cvds).

World Health Organisation. 2023. Hypertension. Accessed 2025 11, March https://www.who.int/news-room/fact-sheets/detail/hypertension#:~:text=Hypertension%20(high%20blood%20pressure)%20is,get%20your%20blood%20pressure%20checked.

Wu, X., W. Shuai, C. Chen, X. Chen, C. Luo, Y. Chen, Y. Shi, Z. Li, X. Lv, C. Chen, et al. 2023. Rapid screening for autoimmune diseases using fourier transform infrared spectroscopy and deep learning algorithms. *Frontiers in Immunology* 14:1328228. doi:10.3389/fimmu.2023.1328228.

Zuccotti, G., and L. Sato. 2011. Malpractice risk in ambulatory settings an increasing and underrecognised problem. *JAMA* 305 (23):2464–5. doi:10.1001/jama.2011.858.